



# CHORUS

This is the accepted manuscript made available via CHORUS. The article has been published as:

## Turbulence generation during the head-on collision of Alfvénic wave packets

O. Pezzi, F. Malara, S. Servidio, F. Valentini, T. N. Parashar, W. H. Matthaeus, and P. Veltri

Phys. Rev. E **96**, 023201 — Published 7 August 2017

DOI: [10.1103/PhysRevE.96.023201](https://doi.org/10.1103/PhysRevE.96.023201)

# Turbulence generation during the head-on collision of Alfvénic wave packets

O. Pezzi<sup>1</sup>, F. Malara<sup>1</sup>, S. Servidio<sup>1</sup>, F. Valentini<sup>1</sup>, T.N. Parashar<sup>2</sup>, W.H. Matthaeus<sup>2</sup> and P. Veltri<sup>1</sup>

<sup>1</sup>*Dipartimento di Fisica, Università della Calabria, 87036 Rende (CS), Italy.*

<sup>2</sup>*Department of Physics and Astronomy, University of Delaware, Newark DE 19716, USA.*

(Dated: July 20, 2017)

The description of the Moffatt & Parker problem recently revisited by O. Pezzi et al. [O. Pezzi et al., *The Astrophys. Journal* **834**, 166 (2017)] is here extended by analyzing the features of the turbulence produced by the interaction of two colliding Alfvénic wave packets in a kinetic plasma. Although the approach based on the presence of linear modes features is still helpful in characterizing some low-energy fluctuations, other signatures, which go beyond the pure linear modes analysis, are recovered, such as the significant weakening of clear dispersion relations and the production of zero frequency fluctuations.

PACS numbers:

## I. INTRODUCTION

The main mechanism of turbulence is the nonlinear coupling among fluctuations, which transfers energy to different spatial scales, thus generating the turbulence spectrum (e.g., [1]). In the ideal incompressible Magneto-hydrodynamics (MHD), where fields are often expressed in terms of the Elsässer variables  $\mathbf{z}^{\pm} = \mathbf{u} \pm \mathbf{b}/(4\pi\rho)^{1/2}$  ( $\mathbf{u}$ ,  $\mathbf{b}$  and  $\rho$  being the velocity, magnetic field and density, respectively) [2], a peculiar aspect is that nonlinear couplings can only take place between  $\delta\mathbf{z}^+$  and  $\delta\mathbf{z}^-$  fluctuations. In this context, Moffatt [3] and Parker [4] considered the problem of the collision of two large-amplitude spatially localized Alfvén wave packets, oppositely propagating along the background magnetic field  $\mathbf{B}_0$ , which can be seen as  $\mathbf{z}^+$  and  $\mathbf{z}^-$  perturbations. Wave packets propagate undistorted until overlapping, when they start being modified by nonlinear interactions. Then, wave packets eventually separate and propagate once again undisturbed without further interactions. The interaction between oppositely propagating Alfvénic packets has been considered as the “building block” of nonlinear phenomena taking place in incompressible MHD turbulence [5–10]. The relevance of this phenomenon is also due to the fact that Alfvénic perturbations represent the main component of fluctuations in weakly compressible natural plasmas, as directly measured in the fast streams of solar wind [11, 12] and inferred in the solar corona by remote sensing observations [13–16].

However, the incompressible approximation is often not fully adequate, since it neglects, obviously compressions, but also dispersion and kinetic effects. Indeed, although many intervals of solar wind are highly Alfvénic [17, 18], small density variations and a small parallel magnetic field variance are found, as in the often-quoted 5:4:1 variance ratio [11]. Moreover, at smaller scales near the ion inertial scale, kinetic properties are observed, such as spectral steepening [12, 19], dispersive wave effects [20–22], temperature anisotropy, beams and other distortions of the proton velocity distribution function (VDF) [23–30]. These considerations place the problem of the collision of Alfvén wave packets in a much more complex

framework.

In two previous papers [31, 32] (hereafter Paper I and II), we revisited the collision of two large-amplitude Alfvénic wave packets by means of compressible MHD, Hall MHD and hybrid Vlasov-Maxwell (HVM) numerical simulations. Results showed a dynamics more complex than that envisaged by Moffatt and Parker in the ideal incompressible MHD case: (i) the complexity of structures produced by nonlinear interactions makes it difficult to determine whether wave packets are fully separated after their collision; (ii) the time behavior of several integral quantities is different from that expected in the ideal incompressible MHD case; (iii) a tendency has been found to build up nearly isotropic spectra, with slope about  $\sim -5/3$ , in the plane almost perpendicular to  $\mathbf{B}_0$ .

A similar problem, concerning the interaction of non-localized moderate-amplitude Alfvén waves at spatial scales comparable with the ion inertial length, has been approached within the weak turbulence framework [33]; moreover gyro-kinetic simulations [34] and laboratory experiments [35–37] have been performed in a similar context. This approach is often based on the assumption of small-amplitude fluctuations and describes turbulence in terms of weakly nonlinear couplings among waves, each belonging to a well-defined propagating mode and maintaining its own distinctive properties (e.g., dispersion relation, etc). The theory of weak turbulence in plasmas has been widely studied within MHD [8, 38], including dispersive effects [39] and also for high-frequency waves [40–42]. Moreover, within this framework, properties concerning the Landau damping of a kinetic Alfvén wave (KAW) or its absorption in an inhomogeneous plasma have been investigated in detail [43–45]. Strong and weak turbulence theories may be viewed as complementary [46, 47], and there is a debate on the applicability of a “wave approach” to describe, for instance, turbulence in the solar wind [48–54]. In the present paper we intend to give further contributions to these fundamental issues.

In the large-amplitude packets collision considered here, the ratio between the nonlinear time  $\tau_{nl} = \Delta/u$  and characteristic wave-packet collision time  $\tau_{coll} = \Delta/V$  is about  $1/2$  (where  $\Delta$ ,  $u$  and  $V$  are respectively the

wave packet width, the perturbation amplitude and the in-plane propagation speed). This indicates that wave packets are significantly modified by nonlinear couplings also in a single collision. The purpose of the present paper is to give some insights concerning the kind of interactions that occur between the packets and to analyze, in particular, the fluctuations generated by the collision in terms of properties associated either with linear modes, or with turbulence. Signatures of localized waves have been also recovered in a fully turbulent scenario driven by the Kelvin-Helmholtz instability [55]. Here we show that wave-like activity, characterized by the presence of linear plasma mode features, diminishes in favor of turbulence even if one starts with Alfvénic wave packets. In particular, we point out that some fluctuations generated by nonlinear interactions display polarization and correlation properties typical of linear modes. However, after the collision, the frequency-wavenumber branches appear significantly broadened and tend to build up quasi-stationary structures.

## II. NUMERICAL APPROACH AND INITIAL CONDITION

Here we numerically solve the hybrid Vlasov-Maxwell (HVM) system of equations for a quasi-neutral plasma composed of kinetic, collisionless protons and fluid Maxwellian electrons [24]. The phase space configuration is  $2.5D-3V$ , which means that all the vector components are retained but they depend only on two spatial coordinates  $\mathbf{x} = (x, y)$ . Dimensionless HVM equations are:

$$\partial_t f + \mathbf{v} \cdot \nabla f + (\mathbf{E} + \mathbf{v} \times \mathbf{B}) \cdot \nabla_{\mathbf{v}} f = 0 \quad (1)$$

$$\mathbf{E} - d_e^2 \Delta \mathbf{E} = -\mathbf{u}_e \times \mathbf{B} - \frac{\nabla P_e}{n} +$$

$$\frac{d_e^2}{n} [\nabla \cdot \boldsymbol{\Pi} + n \mathbf{u} \times \mathbf{B} + \nabla \cdot (n(\mathbf{u}\mathbf{u} - \mathbf{u}_e \mathbf{u}_e))] \quad (2)$$

$$\partial_t \mathbf{B} = -\nabla \times \mathbf{E} \quad ; \quad \nabla \times \mathbf{B} = \mathbf{j} \quad (3)$$

where  $f = f(\mathbf{x}, \mathbf{v}, t)$  is the proton distribution function,  $\mathbf{E}(\mathbf{x}, t)$  is the electric field,  $\mathbf{B}(\mathbf{x}, t) = \mathbf{B}_0 + \mathbf{b}(\mathbf{x}, t)$  is the total magnetic field and  $\mathbf{j} = \nabla \times \mathbf{B}$  is the total current density. Proton density  $n(\mathbf{x}, t)$  and mean velocity  $\mathbf{u}(\mathbf{x}, t)$  are obtained as velocity moments of the proton distribution function  $f$ . Moreover, a quasi-neutrality condition ( $n = n_p = n_e$ ) and an isothermal equation of state for the electron pressure  $P_e$  are assumed. To prevent numerical instabilities electron inertia effects have been considered in Ohm's law using an electron to ion mass ratio  $m_e/m_p = d_e^2 = 0.01$  (being  $d_e$  the electron skin depth), while no external resistivity has been imposed. Since the scale associated with  $d_e$  is almost at the limit of the accessible scales of our simulation, we can reasonably expect that the present value of mass ratio does not influence the results presented here, which occur on scales much larger than  $d_e$ . In Eqs. (1)–(3) time, velocities, lengths and

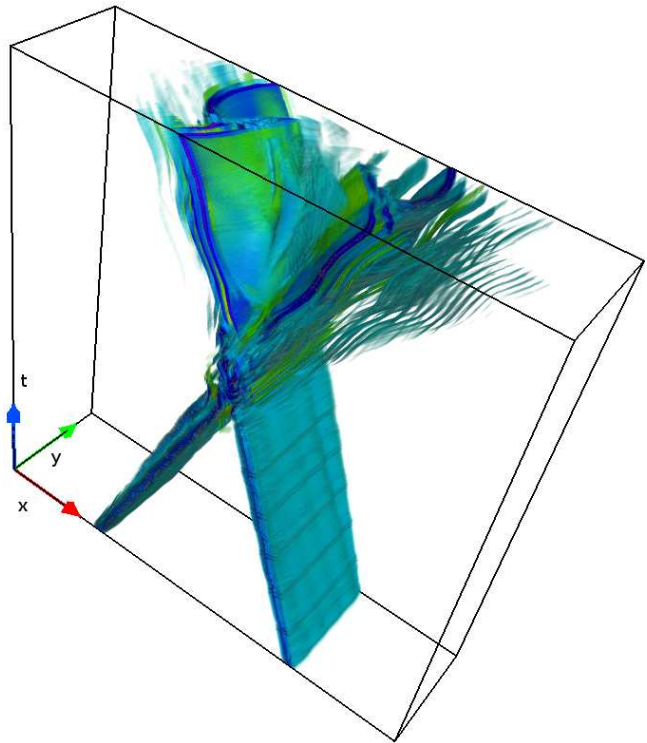


FIG. 1: (Color online) Space-time representation of Alfvénic packets collision by means of the iso-surfaces of the current density  $j_z(x, y, t)$ .

masses are scaled to the inverse ion cyclotron frequency  $\Omega_{cp}^{-1}$ , to the Alfvén speed  $c_A$ , to the proton skin depth  $d_p = c/\omega_{pp} = c_A/\Omega_{cp}$  (being  $c$  the light speed and  $\omega_{pp}$  the proton plasma frequency) and to the proton mass  $m_p$ , respectively. For the sake of simplicity, all the quantities will be scaled as prescribed above. Note that, since here we focus on the HVM simulation, the normalizations are different from the ones adopted in Paper I and II. A detailed description of the numerical method employed to solve Eqs. (1)–(3) can be found in Ref. [24].

Eqs. (1)–(3) are integrated in a double periodic box  $D(x, y) = [0, L_x] \times [0, L_y]$ , being  $L_x = 256$  and  $L_y = 64$ , which has been discretized with  $(N_x, N_y) = (1024, 256)$  points. Each direction of the velocity space is discretized in the region  $v_i = [-5v_{th,p}, 5v_{th,p}]$  with  $N_{v_i} = 51$  mesh points ( $i = x, y, z$ ), where  $\beta_p = 2v_{th,p}^2/c_A^2 = 0.5$  and  $v_{th,p}^2 = k_B T_p/m_p$  is the proton thermal speed. Boundary conditions in the velocity domain assume  $f = 0$  for  $|v_i| > 5v_{th,p}$ .

The background magnetic field  $\mathbf{B}_0$  is mainly perpendicular to the  $x-y$  plane:  $\mathbf{B}_0 = B_0(\sin \vartheta, 0, \cos \vartheta)$ , where  $\vartheta = \cos^{-1}[(\mathbf{B}_0 \cdot \hat{\mathbf{z}})/B_0] = 6^\circ$  and  $B_0 = |\mathbf{B}_0| = 1$  in code units. At  $t = 0$ , the proton VDF is a non-drifting Maxwellian at each spatial point. Then, magnetic  $\mathbf{b}$  and mean velocity  $\mathbf{u}$  perturbations are introduced, while no density perturbations are imposed. As described in Paper I, initial fluctuations consist of two quasi-Alfvénic wave packets with opposite velocity-magnetic field corre-

lation, separated along  $x$ . Since  $B_{0,x} \neq 0$ , wave packets counter-propagate and collide after a time about  $\tau = 600$ . The intensity of the perturbation is  $\langle b \rangle_{rms}/B_0 = 0.2$  and the Mach number is  $M = \langle u \rangle_{rms}/v_{th,p} = 0.4$ . A detailed discussion of the properties of the initial conditions can be found in Paper I.

### III. SIMULATION RESULTS

The evolution of the two wave packets can be easily appreciated in Figure 1, where the shaded surface of the current density  $j_z(x, y, t)$  is reported. The horizontal plane corresponds to  $x - y$  plane, while the temporal evolution is given by the vertical direction. The two wave packets start their motion by approaching each other; then, around  $t = \tau$ , they collide, producing complex current structures. During the collision wave packets interact and change shape, by forming smaller scales fluctuations. As reported in Paper I, magnetic energy spectra tend to become isotropic in the plane, indicating the presence of quasi-perpendicular nonlinear couplings, leading to a slope close to  $-5/3$ . The conservation of the Vlasov invariants in the present simulation is well respected (See Ref. [56] for a detailed discussion). Indeed, the mass, total energy and entropy are respectively conserved up to the 0.1%, 0.5% and 1%.

Here we focus on the description of some significant features which are recovered after the collision. In particular, small-amplitude ripples, which propagate almost purely along  $x$ , appear in front of each wave packet. Moreover, at the center of the spatial domain, some vortical current sheet structures are also present and can be clearly appreciated looking the temporal evolution of  $j_z(x, y, t)$ , which is showed in the Supplementary Material [57].

To understand the physical mechanism driving the production of these secondary small-amplitude ripples, whose wavelength is  $\simeq 5.9$ , Fig. 2(a) reports the evolution of  $|\mathbf{B}|(x, y_0, t^*)$  (solid black) and  $n(x, y_0, t^*)$  (dot-solid red) as a function of  $x$ , zoomed in the region

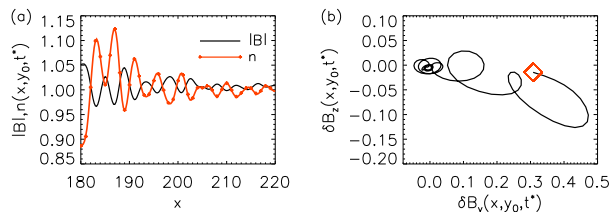


FIG. 2: (Color online) (a) Shape of  $|\mathbf{B}|$  (solid black) and  $n$  (dot-solid red) as a function of  $x$  in the region  $x = [180, 220]$ , for  $y = y_0 = 12$  and  $t = t^* = 1020$ . (b) Hodogram of  $\delta B_z(x, y_0, t^*)$  as a function of  $\delta B_y(x, y_0, t^*)$  for  $x = [180, 220]$ ,  $y = y_0 = 12$  and  $t = t^* = 1020$ . The red square indicates the initial  $x$  point  $x = 180$ .

$x = [180, 220]$  (where these disturbances are present) for  $y = y_0 = 12$  and at  $t = t^* = 1020$ . Density  $n$  and  $|\mathbf{B}|$  fluctuations are anti-correlated, this being typical of Kinetic Alfvén waves and slow magnetosonic modes [22, 58, 59]. In order to differentiate between the two waves branches, we study their polarization by making the hodogram of two magnetic field components [58]. Figure 2 (b) reports the hodogram of  $\delta B_z(x, y_0, t^*)$  as a function of  $\delta B_y(x, y_0, t^*)$ , in the region  $x = [180, 220]$  for  $y = y_0 = 12$  and at  $t = t^* = 1020$ . The red square in Fig. 2 (b) reports the initial point  $x = 180$ . The hodogram shows a clock-wise rotation with increasing  $x$ , that is compatible only with KAWs or fast magnetosonic waves. We finally computed the propagation speed of these fluctuations, finding that this, too, is compatible with the KAWs propagation speed. Therefore, based on these three signatures (correlations, polarization and propagation speed), we conclude that these small-amplitude fluctuations are compatible with KAWs. The presence of these fluctuations is a byproduct of the wave packets interaction: since initial disturbances are mainly Alfvénic, the energy is transferred along the Alfvén wave branch, thus generating these KAW-like ripples.

A description of the system solely in terms of linear plasma mode features is, however, restrictive and the small-amplitude KAWs are just one element of a more complex scenario. Indeed, since  $\tau_{nl}/\tau_{coll} < 1$ , features typical of a turbulent regime may be also reached. To point out that the picture is actually more complex, we performed the following analysis. We selected two temporal windows of duration  $T \simeq 300$  (about 600 time steps), before (I) and after (II) the wave packets collision. In both windows, the magnetic energy  $E_b(\mathbf{x}, t) \simeq \delta \mathbf{B}^2$  is quite stationary. This allows us to implement a full spatio-temporal Fourier transform of  $E_b(\mathbf{x}, t)$  to obtain  $E_b(\mathbf{k}, \omega)$ , thus providing the magnetic energy distribution in the spectral space  $\omega - \mathbf{k}$ . We should remark that the  $\omega$  resolution in our case ( $\Delta\omega = 2\pi/T \approx 2 \times 10^{-2}$ ) is significantly finer than the value recovered through spacecraft measurements [51–54].

Fig. 3 reports the contour plots of  $E_{b,y}(k_x, \omega) = \langle E_b(\mathbf{k}, \omega) \rangle_{k_y}$  (left) and  $E_{b,x}(k_y, \omega) = \langle E_b(\mathbf{k}, \omega) \rangle_{k_x}$  (right) in region I (top) and II (bottom). Before the interaction, the energy  $E_{b,y}(k_x, \omega)$  is recovered mostly at relatively larger scales and is distributed in two branches of waves: Alfvénic (smaller phase speed) and fast magnetosonic (larger phase speed). Note that, since the background magnetic field is quasi-perpendicular to the propagation plane, the Alfvén speed projected onto the  $x - y$  plane is much smaller compared to the Fast magnetosonic phase speed. The coexistence of different waves branches before the main interaction of the two wave packets confirms that our initial perturbations are not purely Alfvénic packets but also include some compressive fluctuations. Some Bernstein fluctuations are also present along the fast waves branch at high frequencies. The energy  $E_{b,x}(k_y, \omega)$  is significantly peaked around  $\omega \approx 0$  at larger wavelength.

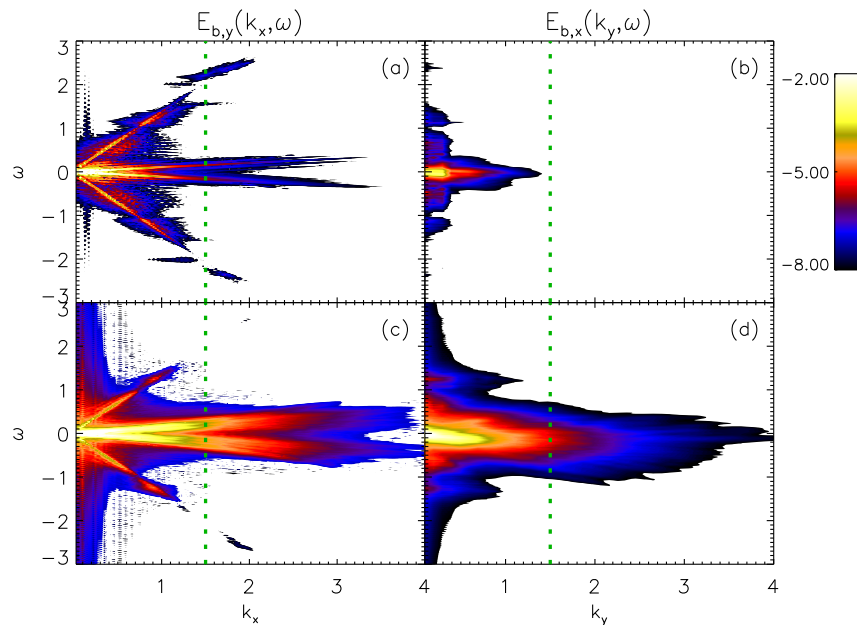


FIG. 3: (Color online) Contour plots of  $E_{b,y}(k_x, \omega) = \langle E_b(\mathbf{k}, \omega) \rangle_{k_y}$  (left) and  $E_{b,x}(k_y, \omega) = \langle E_b(\mathbf{k}, \omega) \rangle_{k_x}$  (right) in region I (before collision, top) and in region II (after collision, bottom). The green dashed lines indicate the wavenumber  $k^* = 1.5$ , at which the cuts reported in Fig. 4 have been performed.

The magnetic energy distribution changes after the wave packet collision. First, smaller spatial scales are populated, as can be easily appreciated in Fig. 3 (c–d), due to the nonlinear couplings which transfer energy towards larger wave number. However, the energy distribution is significantly spread in the  $\omega - k$  space and does not rigidly follow the standard dispersion relations: a cone-like region is populated along the  $k_x$  direction, while a wide blob, peaked at  $\omega = 0$ , is covered in the  $k_y$  direction. Hence, the presence of dispersion relations is significantly weakened after a single collision thus suggesting that turbulence is fundamental for describing the interaction of colliding wave packets. We expect that the dynamics would be even closer to a fully developed turbulent scenario if wave packets could interact several times or for a longer time period.

Figure 4 reports the profile of  $E_{b,y}(k_x = k^*, \omega)$  as a function of  $\omega$  and at a given  $k_x = k^* = 1.5$ , while the inset of Fig. 4 reports  $E_{b,x}(k_y = k^*, \omega)$  as a function of  $\omega$  and at a given  $k_y = k^* = 1.5$ . The range of  $\omega$  in Fig. 4 has been opportunely chosen to focus on Alfvénic fluctuations. Dot-solid red and solid black lines in Fig. 4 refer to the temporal windows before (I) and after (II) the wave packets collision, respectively. Fig. 4 is essentially a cut of Figs. 3 at a given wavenumber, indicated with a green dashed line. Clearly, the growth of the amplitude of  $E_{b,x}(k_y = k^*, \omega)$  after the wave packets collision is due to the fact that a bigger amount of energy is present at  $k_y = k^* = 1.5$  due to the presence of nonlinear couplings which transfer the energy towards large wavenumbers.

Before the collision (dot-solid red line), the energy is

constrained in a relatively narrow band whose width is about few  $\omega_0 \simeq 2\pi/T$ . After the wave packets interaction (solid black line), the energy is instead significantly spread and the populated band width increases by a factor 5. The broadening of the dispersion relation suggests the presence of nonlinear turbulent couplings, whose explanation may be compatible with weak turbulence theory (nonlinear shift of the waves frequency) [60], either with strong turbulence theory (absence of dispersion relation). Moreover, in our simulation, the energy associated with  $\omega \approx 0$  fluctuations significantly increases after the wave packets collision, as it can be appreciated in Fig. 3(c–d) and in Fig. 4, thus suggesting the production of quasi-stationary turbulent structures. Note that the energy distribution shown in the inset of Fig. 4 is peaked at  $\omega \approx 0$  as also recovered in several solar wind observations [51–54].

#### IV. CONCLUSIONS

Here we described the interaction of two colliding Alfvénic wave packets by means of hybrid kinetic Vlasov-Maxwell simulations. We characterized the wave packets' collision by analyzing the features which can be explained in terms of a linear modes approach and the signatures typical of a turbulent regime. Indeed, since the ratio of nonlinear time to overlap/collision time suggests the presence of a turbulent regime, it is interesting to study which linear mode features persist into a turbulent scenario and, on the other hand, which characteristics are

definitively lost. A wave-like analysis, based on polarization and correlation, is still useful to characterize small-amplitude fluctuations that are found to be associated with KAW-like disturbances. However, signatures of a turbulent dynamics are also observed. In particular, i) the energy in the  $\omega - k$  plane is spread after the wave packets' collision and the presence of dispersion relations is, in general, weakened; ii) the energy contained in the  $\omega \approx 0$  fluctuations becomes dominant, thus suggesting the production of quasi-stationary current structures.

### Acknowledgments

Research is supported by NSF AGS-1460130 (SHINE), and NASA grants NNX14AI63G (Heliophysics Grand-challenge Theory), and the Solar Probe Plus science team (ISOIS/SWRI subcontract No. D99031L), and Agenzia Spaziale Italiana under the contract ASI-INAF 2015-039-R.O. "Missione M4 di ESA: Partecipazione Italiana alla fase di assessment della missione THOR". Kinetic numerical simulations here discussed have been run on the Fermi parallel machine at Cineca (Italy), within the

ISCRA-C project IsC37-COLALFWP and on the New-ton parallel machine at University of Calabria (Italy).

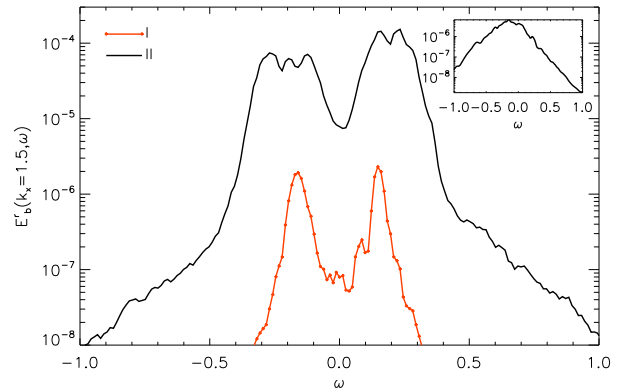


FIG. 4: (Color online) Plot of  $E_{b,y}(k_x = 1.5, \omega)$  as a function of  $\omega$  in the region I (solid black) and II (dot-solid red). The small inset plots  $E_{b,x}(k_y = 1.5, \omega)$  as a function of  $\omega$  in the region II.

- 
- [1] U. Frisch, *Turbulence*, Cambridge University Press, (1995).
- [2] W.M. Elsässer, Phys. Rev. **79**, 183 (1950).
- [3] H.K. Moffatt, *Field Generation in Electrically Conducting Fluids*, (Cambridge University Press, 1978).
- [4] E.N. Parker, "Cosmical magnetic fields: Their origin and their activity.", (1979).
- [5] M. Dobrowolny, A. Mangeney & P. Veltri, Phys. Rev. Lett. **45**, 144 (1980).
- [6] M. Velli, R. Grappin & A. Mangeney, Phys. Rev. Lett. **63**, 1807 (1989).
- [7] W.H. Matthaeus, G.P. Zank, C.W. Smith & S. Oughton, Phys. Rev. Lett. **82**, 3444 (1999).
- [8] S. Galtier, S.V. Nazarenko, A.C. Newell & A. Pouquet, J. Plasma Phys. **63**, 447 (2000).
- [9] A. Verdini, M. Velli & E. Buchlin, The Astrophys. Journal Letters **700**, L39 (2009).
- [10] C.S. Ng & A. Bhattacharjee, The Astrophys. Journal **465**, 845 (1996).
- [11] J.W. Belcher & L. Davis Jr., J. Geophys. Res. **76**, 3534 (1971).
- [12] R. Bruno & V. Carbone, Living Rev. Solar Phys. **10**, 1 (2013).
- [13] W.H. Matthaeus, G.P. Zank, S. Oughton, D.J. Mullan & P. Dmitruk, The Astrophys. J. Letters **523**, L93 (1999).
- [14] S. Tomczyk, S.W. McIntosh, S.L. Keil, P.G. Judge, T. Schad, D.H. Seeley & J. Edmondson, Science **317**, 1192 (2007).
- [15] S. Tomczyk & S.W. McIntosh, The Astrophys. Journal **697**, 1384 (2009).
- [16] A.K. Srivastava, J. Shetye, K. Murawski, J.G. Doyle, M. Stangalini, E. Sculliom, T. Ray, D.P. Wójcik & B.N. Dwivedi, Sci. Reports **7**, 43147 (2017).
- [17] R. Bruno, R. Bavassano & U. Villante, J. Geophys. Res. **90**, 4373 (1985).
- [18] D.J. McComas, L. Barraclough, H.O. Funsten, J.T. Gosling, E. Santiago-Muñoz, R.M. Skoug, B.E. Goldstein, M. Neugebauer, P. Riley & A. Balogh, J. Geophys. Res. **105**, 419 (2000).
- [19] O. Alexandrova, V. Carbone, P. Veltri & L. Sorriso-Valvo, The Astrophys. Journal **674**, 1153 (2008).
- [20] F. Sahraoui, S. Galtier & G. Belmont, J. Plasma Phys. **73**, 723 (2007).
- [21] S.P. Gary, S. Saito & Y. Narita, The Astrophys. Journal **716**, 1332 (2010).
- [22] J.V. Hollweg, J. Geophys. Res. **104**, 14811 (1999).
- [23] E. Marsch, Living Rev. Sol. Phys. **3**(1), 1–100 (2006).
- [24] F. Valentini, P. Trávníček, F. Califano, P. Hellinger & A. Mangeney, J. Comput. Phys. **225**(1), 753–770 (2007).
- [25] F. Valentini, D. Perrone & P. Veltri, The Astrophys. Journal **739**, 54 (2011).
- [26] S. Servidio, F. Valentini, F. Califano & P. Veltri, Phys. Rev. Lett. **108**(4), 045001 (2012).
- [27] D. Perrone, F. Valentini, S. Servidio, S. Dalena & P. Veltri, The Astrophys. Journal **762**, 99 (2013).
- [28] F. Valentini, S. Servidio, D. Perrone, F. Califano, W.H. Matthaeus & P. Veltri, Phys. Plasmas **21**, 082307 (2014).
- [29] S. Servidio, F. Valentini, D. Perrone, A. Greco, F. Califano, W.H. Matthaeus & P. Veltri, J. Plasma Phys. **81**(1), 325810107 (2015).
- [30] J. He, C. Tu, E. Marsch, C.H.K. Chen, L. Wang, Z. Pei, L. Zhang, C.S. Salem & S.D. Bale, The Astrophys. Journal Letters **813**, L30 (2015).
- [31] O. Pezzi, T.N. Parashar, S. Servidio, F. Valentini, C.V. Vásconez, Y. Yang, F. Malara, W.H. Matthaeus & P. Veltri, The Astrophys. Journal **834**, 166 (2017).
- [32] O. Pezzi, T.N. Parashar, S. Servidio, F. Valentini, C.V. Vásconez, Y. Yang, F. Malara, W.H. Matthaeus & P.

- Veltri, J. *Plasma Phys.* **83**, 905830105.
- [33] G.G. Howes & K.D. Nielson, *Phys. Plasmas* **20**, 072302 (2013a).
- [34] K.D. Nielson, G.G. Howes & W. Dorland, *Phys. Plasmas* **20**, 072303 (2013).
- [35] G.G. Howes, K.D. Nielson, D.J. Drake, J.W.R. Schroeder, F. Skiff, C.A. Kletzing & T.A. Carter, *Phys. Plasmas* **20**, 072304 (2013b).
- [36] D.J. Drake, J.W.R. Schroeder, G.G. Howes, C.A. Kletzing, F. Skiff, T.A. Carter & D.W. Auerbach, *Phys. Plasmas* **20**, 072901 (2013).
- [37] D.J. Drake, G.G. Howes, J.R. Rhudy, S.K. Terry, T.A. Carter, C.A. Kletzing, J.W.R. Schroeder & F. Skiff, *Phys. Plasmas* **23**, 022305 (2016).
- [38] S. Sridhar & P. Goldreich, *The Astrophys. Journal* **432**, 612 (1994).
- [39] S. Galtier, *J. Plasma Phys.* **72**, 712 (2006).
- [40] P.H. Yoon, L.F. Ziebell, R. Gaelzer & J. Pavan, *Phys. Plasmas* **19**, 102303 (2012).
- [41] P.H. Yoon, *Phys. Plasmas* **22**, 082309 (2015a).
- [42] P.H. Yoon, *Phys. Plasmas* **22**, 082310 (2015b).
- [43] A. Hasegawa & L. Chen, *Phys. Fluids* **19**, 1924–1934 (1976).
- [44] E.A. Frieman & L. Chen, *Phys. Fluids* **25**, 502–508 (1982).
- [45] L. Rudakov, M. Mithaiwala, G. Ganguli & C. Crabtree, *Phys. Plasmas* **18**, 012307 (2011).
- [46] R. Meyrand, S. Galtier & K.H. Kiyani, *Phys. Rev. Lett.* **116**, 105002 (2016).
- [47] P. Goldreich & S. Sridhar, *The Astrophys. Journal* **438**, 763 (1995).
- [48] A. Barnes, *J. Geophys. Res.* **84**, 4459 (1979).
- [49] W.H. Matthaeus, S. Oughton, K.T. Osman, S. Servidio, M. Wan, S.P. Gary, M.A. Shay, F. Valentini, V. Roytershteyn, H. Karimabadi and S.C. Chapman, *The Astrophys. Journal* **790**, 155 (2014).
- [50] W.H. Matthaeus, M. Wan, S. Servidio, A. Greco, K.T. Osman, S. Oughton & P. Dmitruk, *Philosophical Transaction of the Royal Society of London* **373**, 20140154 (2015).
- [51] Y. Narita, S.P. Gary, S. Saito, K.H. Glassmeier & U. Motschmann, *Geophys. Res. Lett.* **38**, L05101 (2011).
- [52] O.W. Roberts & X. Li, *Astrophys. J.* **802**, 1 (2015a).
- [53] O.W. Roberts, X. Li & L. Jeska, *Astrophys. J.* **802**, 2 (2015b).
- [54] C. Perschke, Y. Narita, U. Motschmann & K.H. Glesmeier, *Phys. Rev. Lett.* **116**, 125101 (2016).
- [55] H. Karimabadi, V. Roytershteyn, M. Wan, W.H. Matthaeus, W. Daughton, P. Wu, M. Shay, B. Loring, J. Borovksy, E. Leonardis, S.C. Chapman & T.K. Nakamura, *Phys. Plasmas* **20**, 012303 (2013).
- [56] C. Vásconez, F. Valentini, E. Camporeale & P. Veltri, *Phys. Plasmas* **21**, 112107 (2014).
- [57] See Supplementary Material at [URL will be inserted by publisher] for the temporal evolution of  $j_z(x, y, t)$ .
- [58] C. Vásconez, F. Pucci, F. Valentini, S. Servidio, W. Matthaeus, & F. Malara, *Astrophys. J.* **815**, 7 (2015).
- [59] F. Pucci, C.L. Vásconez, O. Pezzi, S. Servidio, F. Valentini, W.H. Matthaeus & F. Malara, *J. Geophys. Res.* **121**, 1024 (2016).
- [60] J.D. Crawford, S. Johnston, A.N. Kaufman & C. Oberman, *Phys. Fluids* **29**, 3219–3229 (1986).